ACS APPLIED MATERIALS & INTERFACES

www.acsami.org Research Article

Surface Basicity of Metal@TiO_2 to Enhance Photocatalytic Efficiency for CO_2 Reduction

Lei Jin, Ehab Shaaban, Scott Bamonte, Daniel Cintron, Seth Shuster, Lei Zhang, Gonghu Li,* and Jie He*

Cite This: ACS Appl. Mater. Interfaces 2021, 13, 38595−38603 Read Online

ACCESS | Metrics & More | Article Recommendations | Supporting Information

ABSTRACT: Photocatalytic reduction of CO_2 to valuable chemical fuels is of broad interest, given its potential to activate stable greenhouse CO_2 using renewable energy input. We report how to choose the right metal cocatalysts in combination with the surface basicity of TiO_2 to enhance their photocatalytic efficiency for CO_2 photoreduction. Uniform ligand-free metal nanoparticles (NPs) of Ag, Cu, Au, Pd, and Pt, supported on TiO_2, are active for CO_2 photoreduction using water as an electron donor. The group XI metals show a high selectivity to CO and Ag/TiO_2 is most active to produce CO at a rate of 5.2 μmol g^{-1} h^{-1}. The group X metals, e.g., Pd and Pt, mainly generate hydrocarbons including methane and ethane, and Pd/TiO_2 is slightly more active in methane production at a rate of 2.4 μmol g^{-1} h^{-1}. The activity of these photocatalysts can be enhanced by varying the surface basicity of TiO_2 with primary amines. However, proton reduction selectivity is greatly enhanced in the presence of amine except amine-modified Ag/TiO_2, which shows an activity enhancement by 2.4 times solely for CO_2 photoreduction as compared to that without amines without switching its selectivity to proton reduction. Using in situ infrared spectroscopy and CO stripping voltammetry, we demonstrate that the improvement of electron density and the low proton affinity of metal cocatalysts are of key importance in CO_2 photoreduction. As a systematic study, our results provide a guideline on the right choice of metals in combination of the surface functionality to tune the photocatalytic efficiency of supported metal NPs on TiO_2 for selective CO_2 photoreduction.

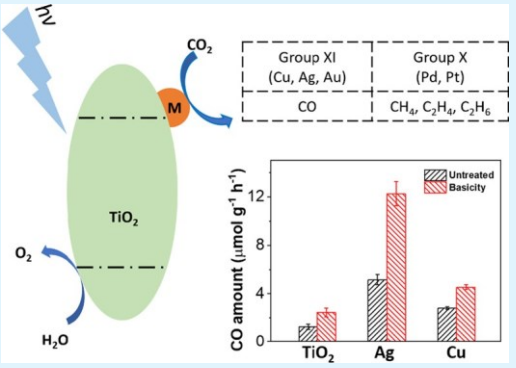

KEYWORDS: CO_2 photoreduction, metal cocatalysts, ligand-free metal, TiO_2, surface basicity, selectivity

1. INTRODUCTION

Effective capture and conversion of CO_2 have attracted considerable attention due to the increasing emission of CO_2 into atmosphere and the rising environmental crisis.[1−5] Photochemical reduction of CO_2 is one of the most attractive approaches to convert CO_2 into valuable chemical fuels using renewable solar energy as the sole energy input.[2,6] The design and synthesis of efficient photocatalysts are of key importance to achieve efficient and selective CO_2 conversion. In a typical photocatalytic process, the band gap excitation of semiconductors under light irradiation provides excited electron−hole pairs. The photogenerated electrons can be utilized to reduce CO_2 on the surface, while the holes can be quenched with green electron donors, e.g., water. Semiconductors with appropriate band gap and conduction band energy have been broadly studied as photocatalysts for CO_2 reduction, such as TiO_2,[7] CdS,[8] ZnO,[9] and g-C_3N_4.[10] Among these photocatalysts, TiO_2 is one of the most extensively studied photocatalysts for CO_2 reduction due to the advantages of high stability, low cost, and low toxicity.[11] However, with semiconductors alone in bulk, photocatalytic efficiency suffered from the fast charge (excited electron−hole pairs) recombination.

There are a number of synthetic strategies proposed in previous studies to address the charge recombination in semiconductors. Controlled synthesis of semiconductors in terms of their sizes[12] and/or porosity[13,14] can enhance their photocatalytic activity because increasing the surface area of semiconductors allows the excited electrons to reach on the surface where photocatalysis occurs. Improving the crystallinity of semiconductors can reduce the charge recombination that is caused by the amorphous defects and low charge mobility in the amorphous domains.[15] In the particular case of TiO_2, the phase engineering to form mixed anatase and rutile phases also have proved to increase the photocatalytic activity due to the charge separation at the phase boundary.[14,16−18] On the other

Received: May 17, 2021
Accepted: July 27, 2021
Published: August 9, 2021

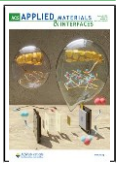

https://doi.org/10.1021/acsami.1c09119
ACS Appl. Mater. Interfaces 2021, 13, 38595−38603

hand, introducing a cocatalyst, like metal nanoparticles (NPs) on semiconductors, offers a very efficient way to relocate/separate excited electrons and avoid charge recombination. When the NPs are grown on the semiconductors, the formation of the Schottky barrier at the metal/semiconductor interface promotes the charge separation and transfers electrons on the surface of metal NPs for the reductive half-reaction.[19,20] Metal cocatalysts tune the product selectivity for CO_2 photoreduction. For example, pure TiO_2 reduced CO_2 to CO as the major product. When Pt was supported on TiO_2, a much higher selectivity to hydrocarbons (CH_4 and C_2H_6) has been reported.[7,21] Metal cocatalysts such as Pd,[22] Au,[23] and Ru[23] have been demonstrated to produce CH_4 and CO when supported on TiO_2. Other metal NPs such as Ag[24] and Cu[25] supported on TiO_2 only show enhanced CO production. Bimetallic nanoalloys like AuCu supported on TiO_2 showed superior activity for photocatalytic CO_2.[26] With the ratio of Au/Cu 1:2, the hybrid photocatalysts were able to produce CH_4 with a selectivity of 97% and it was ~40 times more active compared to pristine TiO_2.

Photoreduction of CO_2 has a sluggish reaction kinetics as it usually involves multiple electron transfers. Previous studies suggest that surface basic sites of catalysts play an important role in various CO_2 reduction reactions like hydrogenation,[27] photoreduction,[28,29] and electroreduction.[30,31] CO_2 as an electrophile can be adsorbed and stabilized through strong interactions with electron-rich Lewis bases. The surface basicity of catalysts can be introduced through many methods like surface ligands,[32,33] oxygen vacancies,[34] and doping.[35] For example, amine-grafted porous silica-like SBA-15 showed enhanced interactions and adsorption with CO_2.[32] The surface amine groups resulted in the ionization of CO_2 to form ionic carbamate and surface-bound carbamate species. TiO_2 modified with primary amines or doped with strong Lewis bases like MgO or amines can significantly improve its activity for CO_2 photoreduction.[28,33] Therefore, controlling the surface basic sites in metal/TiO_2 catalysts is a promising strategy to enhance the catalytic performance of CO_2 reduction. TiO_2 catalysts coated with MgO as an example were 4.3 times more active as compared with the noncoated ones.[28]

We herein report a systematic investigation of the metal/TiO_2 catalysts in photochemical CO_2 reduction to identify the right choice of metal cocatalysts in matching with the surface basicity. Five different metal NPs, including Ag, Cu, Au, Pd, and Pt, were grown on commercial TiO_2 NPs using a deposition−precipitation method. Our syntheses were achieved by electrostatic adsorption of metal salts on TiO_2, followed by reduction using sodium borohydride where no surface ligands were involved. The average diameter of supported NPs is in the range of 1−4 nm. The selectivity and activity difference were compared for CO_2 photoreduction using water as an electron donor. The surface modification on TiO_2 with primary amines improved the catalytic activity for CO_2 photoreduction. However, our results suggested the surface amines were detrimental to the selectivity between CO_2 and proton reductions for most metal nanocatalysts supported on TiO_2. Among various metal cocatalysts, Ag/TiO_2 showed a 2.4-fold kinetic enhancement to reduce CO_2 to CO in the presence of surface amines, while remaining unselective to proton reduction.

2. EXPERIMENTAL SECTION

2.1. Chemicals and Materials. Gold(III) chloride ($HAuCl_4$), sodium tetrachloropalladate (Na_2PdCl_4), potassium hexachloroplatinate (K_2PtCl_6), copper nitrate trihydrate ($Cu(NO_3)_2$ $3H_2O$), (3-aminopropyl)triethoxysilane (APTES), sulfuric acid (H_2SO_4), sodium hydroxide (NaOH), and ethanol were purchased from Sigma-Aldrich. Silver nitrate ($AgNO_3$), sodium borohydride ($NaBH_4$), and succinic anhydride were purchased from Alfa Aesar. Aeroxide TiO_2 P25 was a gift from Evonik Industries. All chemicals were used without further purification. Deionized water (high-Q, Inc. 103S Stills) with a resistivity of >10.0 MΩ was used in all experiments.

2.2. Synthesis of Metal/TiO_2 Catalysts. Metal NPs supported on TiO_2 were synthesized through the deposition−precipitation method as reported previously with some modifications.[36] In a typical synthesis, various metal salts were physically adsorbed on TiO_2 at pH ~ 11.5 under which the surface hydroxyl groups are mostly deprotonated. Taking Ag@TiO_2 as an example, 3.9 mg of $AgNO_3$ (2.5 wt % of Ag relative to TiO_2) was mixed with 100 mg of TiO_2 powder in 15 mL of water. The solution pH was tuned to ~11.5 using ammonia (28% in water). The mixture was sonicated for 10 min and further stirred for 1 h at room temperature. The solution was then heated to 85 °C to evaporate water. The as-resultant powders were redispersed into 10 mL of water, followed by adding 5 mL of freshly prepared ice-cold $NaBH_4$ solution (2 mg mL^{-1}). After stirring for another 1 h at room temperature, the sample was washed with water once and ethanol twice by centrifugation.

2.3. Amine and Acid Modification of M/TiO_2-N and M/TiO_2-COOH. Amine-modified TiO_2 (TiO_2-N) was prepared by surface hydrolysis of APTES on TiO_2.[37] Briefly, 1 g of TiO_2 was first dispersed into 120 mL of ethanol by sonication. Then, 1.5 mL of APTES was added into the solution under stirring. After 10 min, 0.8 mL of ammonia (28% in water) as a catalyst for the hydrolysis of APTES was added into the mixture. The solution was heated to 50 °C and stirred for 8 h under air. The as-prepared sample was collected via centrifugation and washed with ethanol before drying in a vacuum oven.

The surface amines of TiO_2-N were further capped with carboxylic acids (−COOH) to study the role of amines in CO_2 photoreduction. Succinic anhydride was used to cap the surface amines through esterification to prepare TiO_2-COOH.[38] Briefly, 1 g of TiO_2-N was dispersed into 100 mL of anhydrous THF under sonication. Then, 2 g of succinic anhydride was added into the solution under ice bath. The reaction was carried out at 0 °C for 2 h and then kept stirring overnight at room temperature. The final product was washed with ethanol twice before drying under vacuum.

The growth of metals TiO_2N and TiO_2COOH was similar to that of M@TiO_2, while using TiO_2-N and TiO_2-COOH to replace TiO_2.

2.4. Characterization. Transmission electron microscopy (TEM) and high-angle annular dark-field TEM (HAADF-STEM) were carried out on a Talos F200X Atomic Resolution Analytical Microscope. X-ray diffraction (XRD) was recorded on a Bruker D2 phaser. Fourier transform infrared spectroscopy (FT-IR) was conducted using a Bruker Platinum Attenuated total reflection (ATR). Diffuse reflectance infrared Fourier transform spectroscopy (DRIFTS) was examined on a Thermo Nicolet 6700 FT-IR spectrometer. The sample was annealed at 150 °C for 1 h under argon before any test. For CO_2 adsorption, CO_2 balanced with argon was purged for 30 min prior to measurements. For CO adsorption, annealed samples were purged with CO and then argon at room temperature prior to spectrum collection. X-ray photoelectron spectroscopy (XPS) results were collected on a Quantum 2000 Scanning ESCA Microprobe spectrometer with Al Kα radiation. The UV−vis spectra were measured on a Shimadzu UV 2450 equipped with a single monochromatic system. The sample was mixed with barium sulfate to form a uniform pellet. Fluorescence spectroscopy was recorded on a Cary Eclipse fluorescence spectrophotometer. The emission spectrum was collected in the range of 300−425 nm under excitation at 200 nm. The scan rate was 600 nm min^{-1}. In the CO stripping voltammetry, a fixed potential of −0.8 V (vs saturated

https://doi.org/10.1021/acsami.1c09119
ACS Appl. Mater. Interfaces 2021, 13, 38595−38603

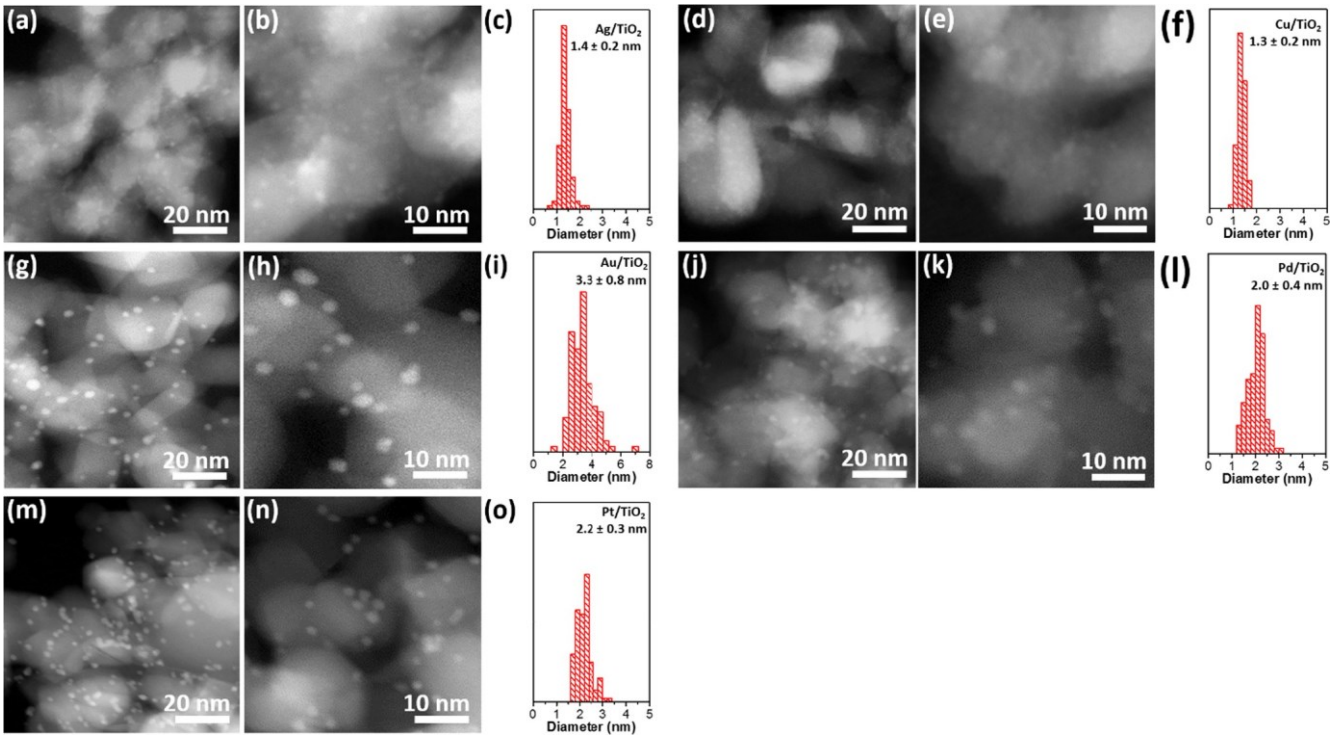

Figure 1. Dark-field TEM images and size distribution of (a−c) Ag/TiO_2, (d−f) Cu/TiO_2, (g−i) Au/TiO_2, (j−l) Pd/TiO_2, and (m−o) Pt/TiO_2.

calomel electrode) was applied to the working electrolyte in 0.1 M NaOH under CO bubbling for 20 min to form the saturated CO adsorption layer. Then, the electrode was transferred to another 0.1 M NaOH electrolyte saturated with N_2. The CO stripping voltammetry was collected at a scan rate of 20 mV s^{-1}.

2.5. Photocatalysis. For photochemical CO_2 reduction, 10 mg of catalyst was dispersed into 10 mL of 0.1 M $NaHCO_3$ in a quartz cell. The mixture solution was degassed and bubbled with CO_2 for 20 min before photoreduction. Then, the cell was irradiated with a 100 W mercury lamp with a filter of 320−390 nm (OmniCure S1500 Spot UV Curing System). The gas products were analyzed on a Shimadzu gas chromatograph (GC-2014) equipped with a packed column (60/80 Carboxen 1000) and a thermal conductive detector (TCD) for H_2 and CO detection. The hydrocarbon products were measured on a HP 6890 GC equipped with a Carboxen 1010 PLOT column and a flame ionization detector (FID). The liquid phase products were analyzed on a Bruker Avance 400 MHz spectrometer after 5 h of reaction.

3. RESULTS AND DISCUSSION

3.1. Synthesis and Characterization of Catalysts. Metal NPs supported on TiO_2 (commercial P25) were prepared via the deposition−precipitation method. The physical adsorption of various metal precursors on TiO_2 was achieved by varying the surface charge of TiO_2. When the pH was above the point of zero charge (~pH 6) of TiO_2, the deprotonation of surface hydroxyl groups would lead to the formation of negatively charged species like $Ti{-}O^-$. At pH ~ 11.5, TiO_2 adsorbed a variety of metal cations through electrostatic interaction as reported previously.[39] Such interaction allows the reasonable dispersity of metal cations on TiO_2, and, therefore, small metal NPs upon reduction. Using sodium borohydride,[36] group X and XI metal NPs, such as Au, Ag, Cu, Pd, and Pt, could be prepared on TiO_2 in the absence of any surfactant. The average sizes of metal NPs are in the range of 1−4 nm supported on spherical TiO_2 NPs (~25 nm in diameter) as confirmed by dark-field scanning transmission electron microscopy (STEM) (Figure 1 and bright-field TEM images in Figure S1).

The XRD pattern shows the mixed rutile (~20%) and anatase (80%) phases of P25 TiO_2 (Figure 2a).[14] No obvious XRD peaks from supported metal NPs can be seen regardless of the type of metal. This is presumably due to the small size of

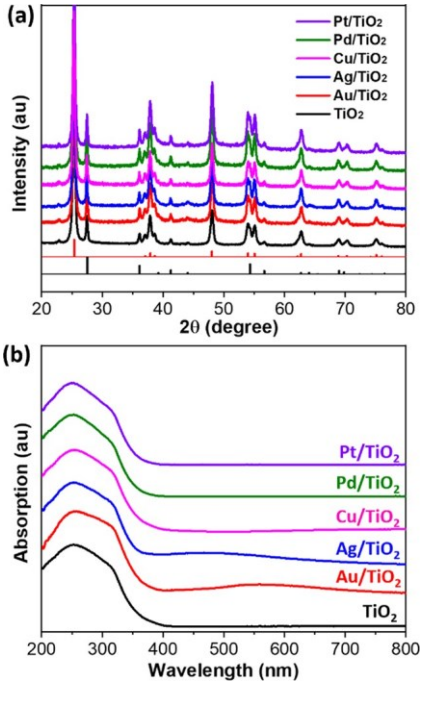

Figure 2. (a) XRD patterns and (b) UV−vis spectra of M/TiO_2 catalysts. The standard patterns are rutile (black, JCPDS 00-001-1292) and anatase (red, JCPDS 00-064-0863) TiO_2 at the bottom of (a).

https://doi.org/10.1021/acsami.1c09119
ACS Appl. Mater. Interfaces 2021, 13, 38595−38603

NPs that usually do not have sharp diffraction peaks.[40] We used a similar method to grow metal NPs on silica (nanopower,10 nm, 99.5%, Sigma-Aldrich) where very broad XRD peaks from metal NPs were observed, indicating the formation of ultrasmall NPs on those oxide supports (Figure S2). The loading amount of all metals estimated from SEM elementary mapping was measured to be ~2 wt %, close to the feeding ratio of metals (Table S1). The diffuse reflectance UV−vis spectra of all metal@TiO_2 are given in Figure 2b. The strong absorption peak in the UV range below 400 nm is from the band gap excitation of TiO_2 (Figure 2b). The weak and broad localized surface plasmon resonance (LSPR) peaks can be seen in the case of Au/TiO_2 (500−600 nm) and Ag/TiO_2 (400−500 nm) due to the existence of NPs with >2 nm.

Surface modification of TiO_2 was carried out to vary the surface basicity since the surface basicity plays an important role in tuning the catalytic performance of CO_2 reduction. We carried out surface modification of TiO_2 first using APTES to generate basic sites (TiO_2-N) prior to the growth of metal NPs to minimize the direct change on the surface of metal NPs. The triethoxysilane moiety of APTES can hydrolyze on the surface of TiO_2, while retaining its primary amine to provide basic sites. Fourier transform infrared spectroscopy (FT-IR) was used to confirm the surface functional groups of TiO_2-N (Figure 3). The peak at ~2927 cm^{-1} was assigned to the C−H

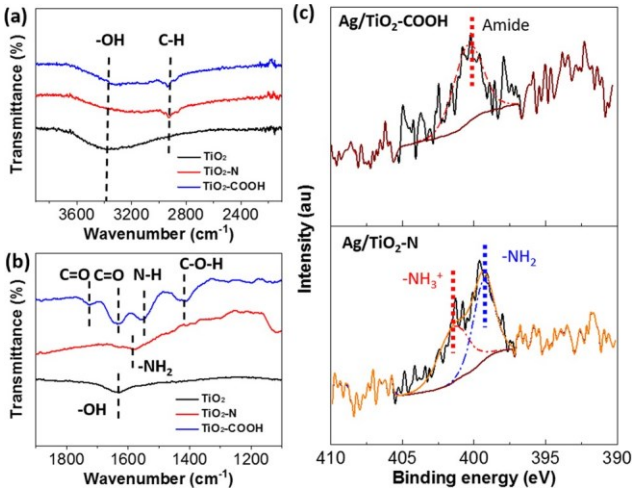

Figure 3. FT-IR spectra of TiO_2, TiO_2-N, and TiO_2-COOH in the ranges of (a) 2200−3800 cm^{-1} and (b) 1900−1100 cm^{-1}. The characteristic feature peaks proved the successful surface modification with basic and acidic sites, respectively. (c) XPS results on the N 1s peaks of Ag/TiO_2-N and Ag/TiO_2-COOH to confirm the grafting of succinic anhydrides.

stretching of $-CH_2-$ species of APTES.[33] A broad peak at around 1582 cm^{-1}, assigned to the bending vibration of $-NH_2$ species,[38] was also observed for TiO_2-N.

As a comparison, the surface amine groups were quenched with succinic anhydride. The capped amine groups existed as amides, while the other acid group of succinic anhydrides remained as carboxylic acids (TiO_2-COOH). After capping, new peaks appeared at 1727 and 1422 cm^{-1} corresponding to the stretching vibration band of free C⊕O and C−O−H.[38] The two peaks at 1635 and 1551 cm^{-1} are assigned to amide I and II bands, known as the C⊕O stretching and N−H bending of amides, respectively.[38] FT-IR spectroscopy confirms the successful surface modification of TiO_2 with basic and acidic sites. The successful surface modification of TiO_2 was further confirmed by XPS as shown in Figure 3c. In the presence of primary amines, Ag/TiO_2-N shows the characteristic peak at 399.3 eV for $-NH_2$ and 401.4 eV for $-NH_3^+$.[41] After converting primary amines to amides with succinic anhydride, the N 1s peak shifted to 400.3 eV.[42] Using this modified TiO_2 as substrate, metal NPs can be synthesized through similar synthetic approaches. For example, with TiO_2-N as the support, uniform metal NPs of Au, Ag, Cu, Pd, and Pt were grown on the surface of TiO_2-N with average diameters of 1−3 nm (Figure S3).

3.2. CO_2 Photoreduction Using Different Metal Cocatalysts on TiO_2. Photoreduction was carried out in a CO_2-saturated $NaHCO_3$ solution (0.1 M) with a light irradiation provided by a mercury lamp with a broad-band filter of 320−390 nm. To better compare the results, 10 mg of catalyst was used in each experiment. As shown in Figure 4a,

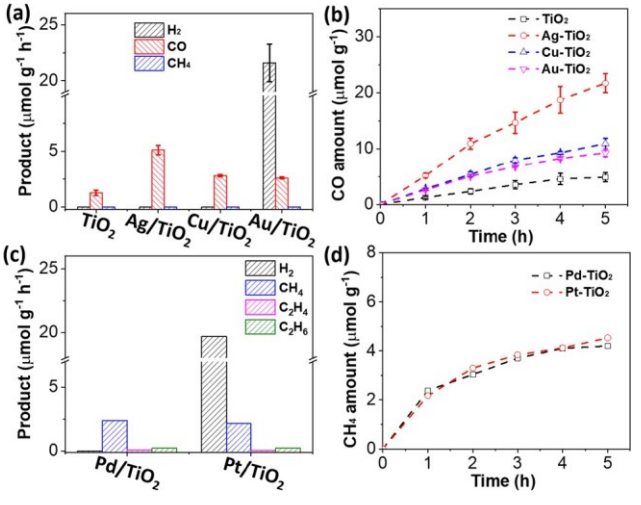

Figure 4. CO_2 reduction performance of TiO_2, Ag/TiO_2, Cu/TiO_2, Au/TiO_2, Pd/TiO_2, and Pt/TiO_2 under UV light (320−390 nm). (a) Average production rate in 1 h. (b) Kinetic curves of CO production of TiO_2, Ag/TiO_2, Cu/TiO_2, and Au/TiO_2 in 5 h. (c) Average production rate in 1 h. (d) Kinetic curves of CH_4 production of Pd/TiO_2 and Pt/TiO_2 in 5 h. The standard deviations are calculated from three independent measurements. Catalytic conditions: 10 mg of catalyst in 10 mL of $NaHCO_3$ (0.1 M). The loading amount of metals on TiO_2 was ~2 wt % (Table S1).

Ag/TiO_2, Cu/TiO_2, and pure TiO_2 showed the CO_2 reduction toward CO, without detectable H_2 or other liquid products. As for the first 1 h, Ag/TiO_2 exhibited the highest CO production of 5.1 ± 0.4 μmol g^{-1} h^{-1}, which is 4 and 1.8 times higher than that of pristine TiO_2 (1.2 ± 0.2 μmol g^{-1} h^{-1}) and Cu/TiO_2 (2.8 ± 0.1 μmol g^{-1} h^{-1}), respectively. Au/TiO_2 showed a CO production rate of 2.6 ± 0.1 μmol g^{-1}; however, a large amount of H_2 of 21.6 ± 2.6 μmol g^{-1} h^{-1} was seen (Figure S4). This suggests that Au as a cocatalyst is less selective for CO_2 reduction. On the other hand, the group X metals, like Pd/TiO_2 and Pt/TiO_2 catalysts, generate hydrocarbons, e.g., CH_4 and C_2H_6. No CO was detected when using Pd/TiO_2 and Pt/TiO_2 (Figure 4c,d). The production rate of CH_4 using Pd/TiO_2 and Pt/TiO_2 was comparable in the range of 2.1−2.4 μmol g^{-1} h^{-1}. This in part is due to strong adsorption of CO intermediates on group X metals where the deep reduction of CO_2 occurs as compared to the group XI metals. Interestingly, we note that Pt/TiO_2 is not selective to reduce CO_2. The

https://doi.org/10.1021/acsami.1c09119
ACS Appl. Mater. Interfaces 2021, 13, 38595−38603

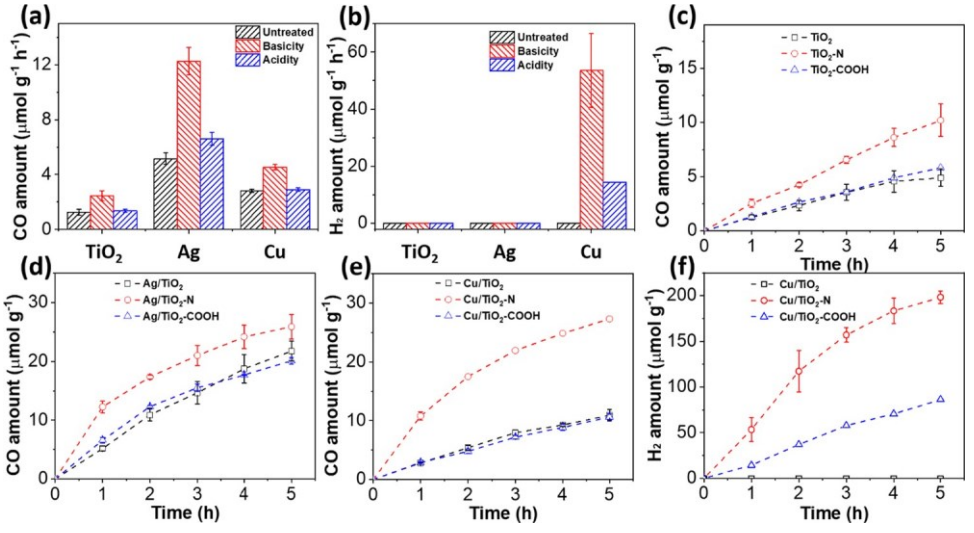

Figure 5. Catalytic performance of TiO_2, Ag/TiO_2, and Cu/TiO_2 with basic and acidic sites in the photocatalytic reduction of CO_2 under UV light (320−390 nm) irradiation. (a) Average production rate of CO in 1 h. (b) Average production rate of H_2 in 1 h. (c−e) Kinetic curves of CO production in 5 h. (f) Kinetic curves of H_2 production in 5 h. H_2 was only detected using Cu/TiO_2 with surface modification. Test conditions: 10 mg of catalyst in 10 mL of $NaHCO_3$ (0.1 M). The loading amount of each metal was ~2 wt % (Table S1).

formation rate of H_2 reached 19.7 μmol g^{-1} h^{-1}, roughly nine times faster than that of CH_4, as a result of the high affinity of protons to Pt.

The kinetic curves of CO and CH_4 are displayed in Figure 4b,d, respectively. The group XI metals are reasonably stable in terms of the formation rate of CO. Ag/TiO_2 exhibited an average CO production rate of 4.3 μmol g^{-1} h^{-1} in 5 h, slightly lower than the initial rate. The difference in the catalytic activity to produce CO between Cu/TiO_2 and Au/TiO_2 is minimum where the kinetic curves almost overlapped (Figure 4b). Pd/TiO_2 and Pt/TiO_2 were less stable as compared to group XI metals (Figures 4d and S5). There is a fast decay in the formation of CH_4 and C_2H_6, while the formation of H_2 over Pt/TiO_2 shows a linear increase along with the reaction time. This presumably is due to the surface coverage of group X metals by the CO intermediates, which blocks the active sites for further CO_2 reduction and only promotes the reduction of protons to form H_2.

3.3. Surface Basicity to Improve CO_2 Photoreduction.

The surface basic sites have proven to enhance the CO_2 reduction performance thermochemically,[41] electrochemically,[31] and photochemically.[43] Surface basic sties show strong bonding to electrophilic CO_2 by forming carbamate species.[32,33] We investigated the impact of the surface basicity of M/TiO_2 catalysts in photochemical CO_2 reduction in terms of their activity and selectivity (competing with protons and among different CO_2 reduction products).[31,44] The surface modification of TiO_2 was carried out prior to the growth of metal NPs to avoid the surface blocking by those molecular species. As a control, we also examined the activity of pristine TiO_2 and TiO_2-N. The photoreduction results are summarized in Figure 5. First of all, for TiO_2 without metal cocatalysts, there is a clear activity enhancement over CO_2 photoreduction. As for the first 1 h, TiO_2-N showed a CO production rate of 2.5 ± 0.4 μmol g^{-1} h^{-1}, approximately two times higher than that of TiO_2. This enhancement completely resulted from the surface basic sites. For metals supported on TiO_2-N, a similar trend was observed. Ag/TiO_2-N produced CO with a rate of 12.3 ± 1.0 μmol g^{-1} h^{-1}, 2.4-fold faster than that of Ag/TiO_2. Cu/TiO_2-N produced CO with a rate of 4.5 ± 0.2 μmol g^{-1} h^{-1}, about 1.6 times more active than Cu/TiO_2. Interestingly, we noted that the activity enhancement was not solely for CO_2 photoreduction. In case of Cu/TiO_2-N, the H_2 production reached 53.5 μmol g^{-1} h^{-1} that was 11.9 times higher than the production rate of CO (Figure 5b). Since the proton reduction to H_2 and the reduction of CO_2 to CO both involve $2e^-$ transfer, the selectivity of protons is 11.9 times more than CO_2. Similar results were observed for Au/TiO_2-N where H_2 was the main reduction product, roughly seven times more than CO (Figure S6). Ag/TiO_2-N is the only photocatalyst that shows basicity-enhanced activity for CO_2 photoreduction, while being not selective to proton reduction. The kinetic curves of TiO_2-N, Ag/TiO_2-N, and Cu/TiO_2-N are summarized in Figure 5c−e. The drop in their activity is likely due to the formation of larger metal NPs during the reaction, as confirmed in Ag/TiO_2-N (see Figure S7).

To further investigate whether the catalytic enhancement of $metal/TiO_2$ is a result of the surface basicity, we capped the surface amines using succinic anhydride (see Section 2 for details). Succinic anhydride converted primary amines to amides, while retaining one −COOH group on the surface of TiO_2. Interestingly, the catalytic performance showed a quick drop very close to its original performance without any surface modification. For example, for TiO_2-COOH, the formation rate of CO is 1.4 ± 0.1 μmol g^{-1} h^{-1}, similar to that of TiO_2. Ag/TiO_2-COOH has a CO formation rate of 6.6 ± 0.5 μmol g^{-1} h^{-1}, close to that of Ag/TiO_2, 5.1 ± 0.4 μmol g^{-1} h^{-1}. The capping of amines also significantly reduced the selectivity of proton reduction. The H_2 generation was also depressed dramatically in Cu/TiO_2-COOH (Figure 5f). The H_2 production of Cu/TiO_2-N was 198.3 μmol g^{-1} over 5 h and it decreased to 86.3 μmol g^{-1} for Cu/TiO_2-COOH. As such, the surface amines on TiO_2 indeed are responsible for the activity enhancement and selectivity control of $metal/TiO_2$ for photocatalytic CO_2 reduction.

Interestingly, both Pd/TiO_2-N and Pt/TiO_2-N showed dramatically enhanced production of C_2H_6 (Figure 6). The production of CH_4 over Pd/TiO_2-N was slightly suppressed, while the production of CH_4 and C_2H_4 over Pt/TiO_2-N was not affected by the amine sites. Pd/TiO_2-N and Pt/TiO_2-N

https://doi.org/10.1021/acsami.1c09119
ACS Appl. Mater. Interfaces 2021, 13, 38595−38603

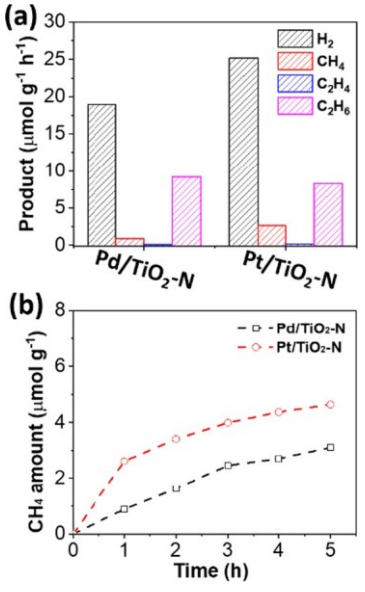

Figure 6. Photocatalytic performance of Pd/TiO_2-N and Pt/TiO_2-N in CO_2 reduction under UV light irradiation. (a) Average production rate of each product in 1 h. (b) Kinetic curves of CH_4 production in 5 h.

generated 9.2 and 8.3 μmol g^{-1} h^{-1} of C_2H_6, respectively. These are close to 40 times higher than Pd/TiO_2 (0.21 μmol g^{-1} h^{-1}) and Pt/TiO_2 (0.23 μmol g^{-1} h^{-1}). However, H_2 production was significantly enhanced for Pd/TiO_2-N, which is comparable with that of Pt/TiO_2-N. These results clearly show that the surface basicity can alter the catalytic performance of metal NP catalysts supported on TiO_2 for CO_2 photoreduction, while it would vary the catalytic selectivity simultaneously.

3.4. Mechanism of CO_2 Photoreduction. The microenvironment of metal/TiO_2 is of critical importance to vary its catalytic activity and selectivity. For CO_2 photoreduction catalyzed by metal/TiO_2, the band gap excitation of TiO_2 accounts for the generation of excited electrons and holes. The first question we address is whether water is the electron donor to replenish the holes, while CO_2 gets reduced on either metal cocatalyst or TiO_2. We used the kinetic isotope effect (KIE) to examine the photooxidation half-reaction. Water as a sacrificial electron donor would be oxidized to form oxygen, known as $2H_2O - 4e^- \rightarrow O_2 + 4H^+$. Water also acts as a proton source to carry out proton-assisted CO_2 reduction. If water is replaced with deuterium oxide (D_2O), the overall rate of CO_2 photoreduction will be varied.[45] Given that deuterium is heavier than the proton, a slower reduction rate would be expected in D_2O. Using Ag/TiO_2 as an example, the CO production rate decreased to 3.2 ± 0.2 μmol g^{-1} h^{-1} in D_2O, as compared to 5.1 ± 0.4 μmol g^{-1} h^{-1} in water (Figure 7). The KIE is 1.6, indicating the presence of O−H bond breakage in photoreduction. The large KIE factor indicates that water participates in CO_2 photoreduction likely to provide electrons and protons to reduce CO_2.

We further examined the electronic states of the metal and TiO_2 surfaces, i.e., whether the surface basicity changed the metal−support interaction.[46] High-resolution Ag 3d and Ti 2p spectra of Ag/TiO_2, Ag/TiO_2-N, and Ag/TiO_2-COOH are given in Figure S8. No significant difference in the binding energy of Ti 2p and Ag 3d among the three samples was observed, suggesting that the bulking electronic structures of

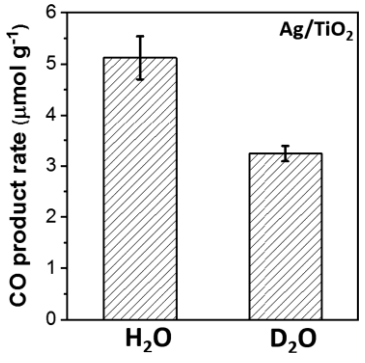

Figure 7. CO production rates of Ag/TiO_2 using D_2O and H_2O as sacrificial electron donors.

Ag and Ti are not varied in the course of surface modification. Therefore, the change in the surface basicity does not vary the metal−support interaction.

With amine modification on TiO_2, the surface basic sites favor the adsorption of electrophilic CO_2 on oxides and possibly on metal catalysts as well.[31] We first used DRIFTS to characterize CO_2 adsorption. Figure 8a shows the DRIFTS

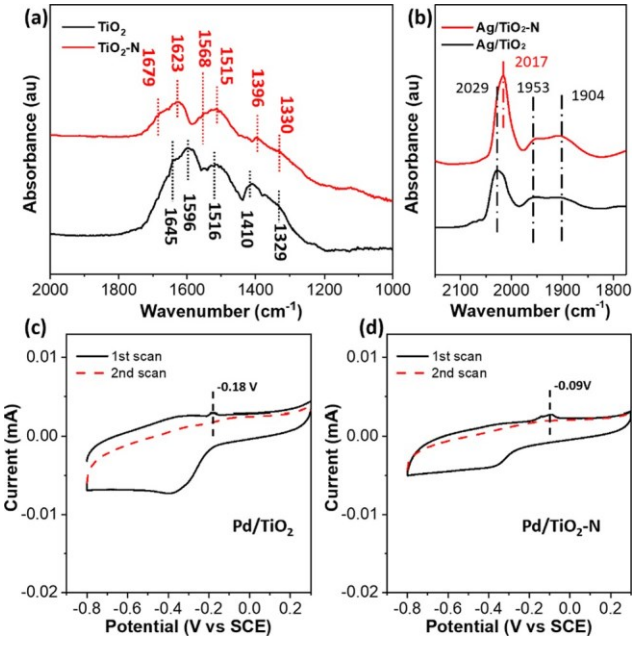

Figure 8. (a) DRIFTS results of CO_2 adsorption on TiO_2 and TiO_2-N. (b) DRIFTS results of CO adsorption on Ag/TiO_2 and Ag/TiO_2-N. (c,d) CO stripping voltammetry of (c) Pd/TiO_2 and (d) Pd/TiO_2-N measured in 0.1 M NaOH.

results of CO_2 adsorption on pristine TiO_2 and TiO_2-N. Without primary amines, TiO_2 after purging with CO_2 has a strong peak at 1645 cm^{-1} assigned to the surface bicarbonate species.[47] Two peaks appearing at 1594 and 1329 cm^{-1} are assigned to bidentate carbonate species on TiO_2.[48] The peaks at around 1516 and 1410 cm^{-1} are attributed to the monodentate carbonate species.[48,49] With surface amines, TiO_2-N also displayed similar carbonate species, which were located at 1515, 1396, and 1330 cm^{-1}. However, a new peak at around 1679 cm^{-1} is seen, likely arising from the carbonyl groups from surface-bound carbamate species in the form of $-NH_2COOH$ or $-NH_3^+$ COO^-.[41] The new peak at 1623

https://doi.org/10.1021/acsami.1c09119
ACS Appl. Mater. Interfaces 2021, 13, 38595−38603

cm^{-1} is presumably from the bending vibration of NH_3^+ species.[41] The CO_2 adsorption confirms the different adsorption modes of CO_2 on TiO_2 in the presence of amines. Although the absolute adsorption cannot be quantified, more binding models of CO_2 are indicative of a stronger affinity and stabilization of CO_2 that is beneficial for better performance.

We further used DRIFTS to monitor the in situ CO_2 photoreduction with trace amount of moisture (Figure S9). Using Ag/TiO_2 as an example, the peak at 1566 cm^{-1} raised dramatically under light irradiation, which refers to monodentate carbonate species.[50] Another peak appeared at 1688 cm^{-1}, which was assigned to surface bicarbonate species.[47] On the contrary, Ag/TiO_2-N exhibited a peak at 1695 cm^{-1}, which was assigned to surface-bound carbamate species.[41] These different surface species formed during the reactions are key to affect the activity and selectivity. The carbamate species in metal/TiO_2-N seems to be favorable for the CO_2 activation and reduction, as seen in the case of Ag/TiO_2-N, Cu/TiO_2-N, and Pd/TiO_2-N. For Cu/TiO_2-N and Pd/TiO_2-N, both samples with a high selectivity to proton reduction showed a new peak around 1700 cm^{-1} for carbonyl groups. Although the assignment of this new peak is unclear, it is possibly the deprotonated form of surface-bound carbamate species. The protons that are also strongly electrophilic can be reduced to form H_2 that competes with CO_2. The formation of these deprotonated carbamate species indicates the reduction of localized protons that varies the overall selectivity.

The surface basicity of TiO_2 can vary the electron density of the supported NPs to vary the affinity of CO_2 to metal NPs. Using CO as a probe molecule, we examined the change of CO vibrational frequency to identify the surface charge density of metal NPs using DRIFTS (Figure 8b). For Ag/TiO_2, there are three new peaks as a result of the CO adsorption on Ag. The peak at 2029 cm^{-1} is assigned to the linear bound (atop sites) CO on Ag(0) and the other two broad peaks at 1953 and 1904 cm^{-1} are from the bridge bound CO. When TiO_2-N was used as the support, a clear shift from 2029 to 2017 cm^{-1} can be seen for the linear bound CO mode.[51,52] Similar results on the DRIFTS spectra of adsorbed CO were observed on Pt and Cu NPs (Figure S10). These results indicate that the metallic NPs become more negatively charged in the presence of surface amines; as such, the binding of electrophilic CO_2 is presumable favorable on metal NPs. In addition, we cross-compared the electronic states of metal NPs using CO stripping voltammetry (Figure 8c−d). The adsorption of CO monolayer, e.g., on Pd, showed different oxidative potentials when modifying the surface of TiO_2 with amines. Pd/TiO_2 has an oxidation peak at −0.18 V (vs saturated calomel electrode) at pH 13, while the oxidation peak shifts to −0.09 V for Pd/TiO_2-N. The positive shift of CO oxidative potentials confirms that the amine functionalization of TiO_2 increases the surface charge density of supported metal NPs.[53]

There are three essential steps in CO_2 photoreduction, including light absorption, charge separation, and the surface catalytic process.[54] In view of our catalysts, we minimize the differences in the band gap of semiconductors and the interfacing of surface ligands on metal NPs. Therefore, the differences in catalytic performance are attributed to the charge separation and catalytic process caused by different supported NPs. Using metal NPs as a cocatalyst allows the efficient charge separation of the band gap excitation of TiO_2. The increase of CO_2 reduction products, i.e., CO from group X metals and hydrocarbon from group XI metals, is mainly attributed to the increase of charge separation, regardless of the surface basicity. Among different metals, Ag is the most active cocatalyst where Ag/TiO_2 is four times more active than TiO_2 and Ag/TiO_2-N is five times more active than TiO_2-N. The surface basicity provided by primary amines shows enhanced affinity to CO_2. The activity of CO_2 photoreduction to CO using group X metals supported on TiO_2 shows ~2-fold increase as compared to those without surface amines. However, other than Ag, the activity enhancement toward proton reduction is much more pronounced in comparison to CO_2 photoreduction. The hydrogen adsorption energy on metals may play a role in the switch of the selectivity. Ag shows the lowest hydrogen adsorption energy among group X and XI metals;[55] therefore, the binding of protons to Ag very unlikely occurs when competing with CO_2. The surface-bound carbamate species are likely responsible to improve the activity of CO_2 photoreduction, given the increase of localized concentration of CO_2, while the deprotonation of those carbamate species likely varies the selectivity of photocatalysts, i.e., increasing proton reduction.

4. CONCLUSIONS

To summarize, we report a systematic study on how the metal cocatalysts and surface basicity improve the photocatalytic efficiency of supported metal cocatalysts on TiO_2 for CO_2 reduction using water as an electron donor. Our key finding is that, although the surface basic sites in the form of amines enhance the activity of metal@TiO_2 photocatalysts, there is a large decrease in the selectivity toward CO_2 reduction over proton reduction for most of the metal cocatalysts other than Ag-supported TiO_2. Using the deposition−precipitation method, ligand-free and ultrasmall metal NPs were grown on commercial TiO_2 powders with different surface functionalities. All metal NPs supported on TiO_2 showed an improved activity for CO_2 photoreduction, while group XI metals varied the reduction products from CO to hydrocarbons. Ag/TiO_2 is the most active photocatalyst to produce CO at a rate of 5.2 $\mu mol\ g^{-1}\ h^{-1}$, four times more active than pristine TiO_2. The group X metals, e.g., Pd and Pt, mainly generated hydrocarbons including methane and ethane and Pd/TiO_2 is slightly more active in methane production at a rate of 2.4 $\mu mol\ g^{-1}\ h^{-1}$. Surface modification with primary amines on TiO_2 showed the activity enhancement regardless of metal cocatalysts. Ag/TiO_2-N was 2.4-fold more active to produce CO as compared to Ag/TiO_2. With surface basic sites, other metals supported on TiO_2 showed different selectivity in comparison with their counterpart without surface modification. The high selectivity toward proton reduction was seen in the cases of Au, Cu, Pd, and Pt. We used DRIFTS and CO stripping voltammetry to confirm the enhanced adsorption of CO_2 and the increase of surface charge density of metal NPs due to the surface basicity on TiO_2. The surface-bound carbamate species on basic sites likely improves the activity. As a systematic comparison, our study provides a general guideline on the choice of metals in combination with the surface functionality to tune the photocatalytic efficiency for CO_2 photoreduction.

ASSOCIATED CONTENT

Supporting Information

The Supporting Information is available free of charge at https://pubs.acs.org/doi/10.1021/acsami.1c09119.

https://doi.org/10.1021/acsami.1c09119
ACS Appl. Mater. Interfaces 2021, 13, 38595−38603

Additional XRD, TEM, photochemical CO_2 reduction results, and DRIFTS spectra (PDF)

AUTHOR INFORMATION

Corresponding Authors

Gonghu Li − Department of Chemistry, University of New Hampshire, Durham, New Hampshire 03824, United States; orcid.org/0000-0002-2924-3597; Email: gonghu.li@unh.edu

Jie He − Department of Chemistry, University of Connecticut, Storrs, Connecticut 06269, United States; Institute of Materials Science, University of Connecticut, Storrs, Connecticut 06269, United States; orcid.org/0000-0003-0252-3094; Email: jie.he@uconn.edu

Authors

Lei Jin − Department of Chemistry, University of Connecticut, Storrs, Connecticut 06269, United States; orcid.org/0000-0002-6070-7863

Ehab Shaaban − Department of Chemistry, University of New Hampshire, Durham, New Hampshire 03824, United States

Scott Bamonte − Department of Chemistry, University of Connecticut, Storrs, Connecticut 06269, United States

Daniel Cintron − Department of Chemistry, University of Connecticut, Storrs, Connecticut 06269, United States

Seth Shuster − Department of Chemistry, University of Connecticut, Storrs, Connecticut 06269, United States

Lei Zhang − Department of Chemistry, University of Connecticut, Storrs, Connecticut 06269, United States

Complete contact information is available at: https://pubs.acs.org/10.1021/acsami.1c09119

Notes

The authors declare no competing financial interest.

ACKNOWLEDGMENTS

J.H. is grateful for the support from the U.S. National Science Foundation under grants 1705566 and 1936228. G.L. acknowledges the support from the U.S. National Science Foundation under grant 1705528. SEM/TEM studies were performed using the facilities in the UConn/FEI Center for Advanced Microscopy and Materials Analysis (CAMMA). This work was also partially supported by the Green Emulsions Micelles and Surfactants (GEMS) Center of the University of Connecticut.

REFERENCES

(1) Chang, X.; Wang, T.; Gong, J. CO_2 Photo-Reduction: Insights into CO_2 Activation and Reaction on Surfaces of Photocatalysts. Energy Environ. Sci. 2016, 9, 2177−2196.

(2) Kumar, B.; Llorente, M.; Froehlich, J.; Dang, T.; Sathrum, A.; Kubiak, C. P. Photochemical and Photoelectrochemical Reduction of CO_2. Annu. Rev. Phys. Chem. 2012, 63, 541−569.

(3) Lewis, N. S.; Nocera, D. G. Powering the Planet: Chemical Challenges in Solar Energy Utilization. Proc. Natl. Acad. Sci. U.S.A. 2006, 103, 15729−15735.

(4) Qiao, J.; Liu, Y.; Hong, F.; Zhang, J. A review of catalysts for the electroreduction of carbon dioxide to produce low-carbon fuels. Chem. Soc. Rev. 2014, 43, 631−675.

(5) Wang, W.; Wang, S.; Ma, X.; Gong, J. Recent Advances in Catalytic Hydrogenation of Carbon Dioxide. Chem. Soc. Rev. 2011, 40, 3703−3727.

(6) Low, J.; Cheng, B.; Yu, J. Surface Modification and Enhanced Photocatalytic CO_2 Reduction Performance of TiO_2: A Review. Appl. Surf. Sci. 2017, 392, 658−686.

(7) Wang, W.-N.; An, W.-J.; Ramalingam, B.; Mukherjee, S.; Niedzwiedzki, D. M.; Gangopadhyay, S.; Biswas, P. Size and Structure Matter: Enhanced CO_2 Photoreduction Efficiency by Size-Resolved Ultrafine Pt Nanoparticles on TiO_2 Single Crystals. J. Am. Chem. Soc. 2012, 134, 11276−11281.

(8) Kuehnel, M. F.; Orchard, K. L.; Dalle, K. E.; Reisner, E. Selective Photocatalytic CO_2 Reduction in Water through Anchoring of a Molecular Ni Catalyst on CdS Nanocrystals. J. Am. Chem. Soc. 2017, 139, 7217−7223.

(9) Núñez, J.; de la Peña O'Shea, V. A.; Jana, P.; Coronado, J. M.; Serrano, D. P. Effect of Copper on the Performance of ZnO and $ZnO_{1-x}N_x$ Oxides as CO_2 Photoreduction Catalysts. Catal. Today 2013, 209, 21−27.

(10) Huang, P.; Huang, J.; Pantovich, S. A.; Carl, A. D.; Fenton, T. G.; Caputo, C. A.; Grimm, R. L.; Frenkel, A. I.; Li, G. Selective CO_2 Reduction Catalyzed by Single Cobalt Sites on Carbon Nitride under Visible-Light Irradiation. J. Am. Chem. Soc. 2018, 140, 16042−16047.

(11) Dimitrijevic, N. M.; Vijayan, B. K.; Poluektov, O. G.; Rajh, T.; Gray, K. A.; He, H.; Zapol, P. Role of Water and Carbonates in Photocatalytic Transformation of CO_2 to CH_4 on Titania. J. Am. Chem. Soc. 2011, 133, 3964−3971.

(12) Azeez, F.; Al-Hetlani, E.; Arafa, M.; Abdelmonem, Y.; Nazeer, A. A.; Amin, M. O.; Madkour, M. The Effect of Surface Charge on Photocatalytic Degradation of Methylene Blue Dye Using Chargeable Titania Nanoparticles. Sci. Rep. 2018, 8, No. 7104.

(13) Mor, G. K.; Shankar, K.; Paulose, M.; Varghese, O. K.; Grimes, C. A. Enhanced Photocleavage of Water Using Titania Nanotube Arrays. Nano lett. 2005, 5, 191−195.

(14) Liu, B.; Luo, Z.; Federico, A.; Song, W.; Suib, S. L.; He, J. Colloidal Amphiphile-Templated Growth of Highly Crystalline Mesoporous Nonsiliceous Oxides. Chem. Mater. 2015, 27, 6173−6176.

(15) Wu, N.; Wang, J.; Tafen, D. N.; Wang, H.; Zheng, J.-G.; Lewis, J. P.; Liu, X.; Leonard, S. S.; Manivannan, A. Shape-Enhanced Photocatalytic Activity of Single-Crystalline Anatase TiO_2 (101) Nanobelts. J. Am. Chem. Soc. 2010, 132, 6679−6685.

(16) Henderson, M. A. A Surface Science Perspective on TiO_2 Photocatalysis. Surf. Sci. Rep. 2011, 66, 185−297.

(17) Kafizas, A.; Wang, X.; Pendlebury, S. R.; Barnes, P.; Ling, M.; Sotelo-Vazquez, C.; Quesada-Cabrera, R.; Li, C.; Parkin, I. P.; Durrant, J. R. Where Do Photogenerated Holes Go in Anatase:Rutile TiO_2? A Transient Absorption Spectroscopy Study of Charge Transfer and Lifetime. J. Phys. Chem. A 2016, 120, 715−723.

(18) Li, H.; Zhang, W.; Pan, W. Enhanced Photocatalytic Activity of Electrospun TiO_2 Nanofibers with Optimal Anatase/Rutile Ratio. J. Am. Ceram. Soc. 2011, 94, 3184−3187.

(19) Liu, B.; Louis, M.; Jin, L.; Li, G.; He, J. Co-Template Directed Synthesis of Gold Nanoparticles in Mesoporous Titanium Dioxide. Chem.−Eur. J. 2018, 24, 9651−9657.

(20) Habisreutinger, S. N.; Schmidt-Mende, L.; Stolarczyk, J. K. Photocatalytic Reduction of CO_2 on TiO_2 and Other Semiconductors. Angew. Chem., Int. Ed. 2013, 52, 7372−7408.

(21) Sorcar, S.; Thompson, J.; Hwang, Y.; Park, Y. H.; Majima, T.; Grimes, C. A.; Durrant, J. R.; In, S.-I. High-Rate Solar-Light Photoconversion of CO_2 to Fuel: Controllable Transformation from C1 to C2 Products. Energy Environ. Sci. 2018, 11, 3183−3193.

(22) Tan, D.; Zhang, J.; Shi, J.; Li, S.; Zhang, B.; Tan, X.; Zhang, F.; Liu, L.; Shao, D.; Han, B. Photocatalytic CO_2 Transformation to CH_4 by Ag/Pd Bimetals Supported on N-Doped TiO_2 Nanosheet. ACS Appl. Mater. Interfaces 2018, 10, 24516−24522.

(23) Kar, P.; Farsinezhad, S.; Mahdi, N.; Zhang, Y.; Obuekwe, U.; Sharma, H.; Shen, J.; Semagina, N.; Shankar, K. Enhanced CH_4 Yield by Photocatalytic CO_2 Reduction Using TiO_2 Nanotube Arrays Grafted with Au, Ru, and ZnPd Nanoparticles. Nano Res. 2016, 9, 3478−3493.

(24) Zhao, C.; Krall, A.; Zhao, H.; Zhang, Q.; Li, Y. Ultrasonic Spray Pyrolysis Synthesis of Ag/TiO_2 Nanocomposite Photocatalysts for Simultaneous H_2 Production and CO_2 Reduction. Int. J. Hydrogen Energy 2012, 37, 9967−9976.
(25) Liu, L.; Gao, F.; Zhao, H.; Li, Y. Tailoring Cu Valence and Oxygen Vacancy in Cu/TiO_2 Catalysts for Enhanced CO_2 Photoreduction Efficiency. Appl. Catal., B 2013, 134−135, 349−358.
(26) Neatu, S.; Maciá-Agulló, J. A.; Concepción, P.; Garcia, H. Gold−Copper Nanoalloys Supported on TiO_2 as Photocatalysts for CO_2 Reduction by Water. J. Am. Chem. Soc. 2014, 136, 15969−15976.
(27) Liu, C.; Guo, X.; Guo, Q.; Mao, D.; Yu, J.; Lu, G. Methanol Synthesis from CO_2 Hydrogenation over Copper Catalysts Supported on MgO-Modified TiO_2. J. Mol. Catal. A: Chem. 2016, 425, 86−93.
(28) Feng, X.; Pan, F.; Zhao, H.; Deng, W.; Zhang, P.; Zhou, H.-C.; Li, Y. Atomic Layer Deposition Enabled MgO Surface Coating on Porous TiO_2 for Improved CO_2 Photoreduction. Appl. Catal., B 2018, 238, 274−283.
(29) Lin, L.-Y.; Nie, Y.; Kavadiya, S.; Soundappan, T.; Biswas, P. N-doped Reduced Graphene Oxide Promoted Nano TiO_2 as a Bifunctional Adsorbent/Photocatalyst for CO_2 Photoreduction: Effect of N Species. Chem. Eng. J 2017, 316, 449−460.
(30) Fang, Y.; Flake, J. C. Electrochemical Reduction of CO_2 at Functionalized Au Electrodes. J. Am. Chem. Soc. 2017, 139, 3399−3405.
(31) Jin, L.; Liu, B.; Wang, P.; Yao, H.; Achola, L. A.; Kerns, P.; Lopes, A.; Yang, Y.; Ho, J.; Moewes, A.; Pei, Y.; He, J. Ultrasmall Au Nanocatalysts Supported on Nitrided Carbon for Electrocatalytic CO_2 Reduction: the Role of the Carbon Support in High Selectivity. Nanoscale 2018, 10, 14678−14686.
(32) Danon, A.; Stair, P. C.; Weitz, E. FTIR Study of CO_2 Adsorption on Amine-Grafted SBA-15: Elucidation of Adsorbed Species. J. Phys. Chem. C 2011, 115, 11540−11549.
(33) Liao, Y.; Cao, S.-W.; Yuan, Y.; Gu, Q.; Zhang, Z.; Xue, C. Efficient CO_2 Capture and Photoreduction by Amine-Functionalized TiO_2. Chem. - Eur. J. 2014, 20, 10220−10222.
(34) Gu, Z.; Yang, N.; Han, P.; Kuang, M.; Mei, B.; Jiang, Z.; Zhong, J.; Li, L.; Zheng, G. Oxygen Vacancy Tuning toward Efficient Electrocatalytic CO_2 Reduction to C_2H_4. Small Methods 2019, 3, No. 1800449.
(35) Li, H.; Li, J.; Thomas, A.; Liao, Y. Ultra-High Surface Area Nitrogen-Doped Carbon Aerogels Derived From a Schiff-Base Porous Organic Polymer Aerogel for CO_2 Storage and Supercapacitors. Adv. Funct. Mater. 2019, 29, No. 1904785.
(36) Mori, K.; Sano, T.; Kobayashi, H.; Yamashita, H. Surface Engineering of a Supported PdAg Catalyst for Hydrogenation of CO_2 to Formic Acid: Elucidating the Active Pd Atoms in Alloy Nanoparticles. J. Am. Chem. Soc. 2018, 140, 8902−8909.
(37) Yang, S.; Feng, X.; Ivanovici, S.; Müllen, K. Fabrication of Graphene-Encapsulated Oxide Nanoparticles: Towards High-Performance Anode Materials for Lithium Storage. Angew. Chem., Int. Ed. 2010, 49, 8408−8411.
(38) Feifel, S. C.; Lisdat, F. Silica Nanoparticles for the Layer-by-Layer Assembly of Fully Electro-Active Cytochrome c Multilayers. J. Nanobiotechnol. 2011, 9, No. 59.
(39) Wong, A.; Liu, Q.; Griffin, S.; Nicholls, A.; Regalbuto, J. R. Synthesis of Ultrasmall, Homogeneously Alloyed, Bimetallic Nanoparticles on Silica Supports. Science 2017, 358, 1427−1430.
(40) Liu, B.; Yao, H.; Song, W.; Jin, L.; Mosa, I. M.; Rusling, J. F.; Suib, S. L.; He, J. Ligand-Free Noble Metal Nanocluster Catalysts on Carbon Supports via "Soft" Nitriding. J. Am. Chem. Soc. 2016, 138, 4718−4721.
(41) Liu, Q.; Yang, X.; Li, L.; Miao, S.; Li, Y.; Li, Y.; Wang, X.; Huang, Y.; Zhang, T. Direct Catalytic Hydrogenation of CO_2 to Formate over a Schiff-Base-Mediated Gold Nanocatalyst. Nat. Commun. 2017, 8, No. 1407,
(42) Zorn, G.; Liu, L.-H.; Arnadóttir, L.; Wang, H.; Gamble, L. J.; Castner, D. G.; Yan, M. X-ray Photoelectron Spectroscopy Investigation of the Nitrogen Species in Photoactive Perfluorophenylazide-Modified Surfaces. J. Phys. Chem. C 2014, 118, 376−383.
(43) Xia, P.; Antonietti, M.; Zhu, B.; Heil, T.; Yu, J.; Cao, S. Designing Defective Crystalline Carbon Nitride to Enable Selective CO_2 Photoreduction in the Gas Phase. Adv. Funct. Mater. 2019, 29, No. 1900093.
(44) Gao, D.; Zhang, Y.; Zhou, Z.; Cai, F.; Zhao, X.; Huang, W.; Li, Y.; Zhu, J.; Liu, P.; Yang, F.; Wang, G.; Bao, X. Enhancing CO_2 Electroreduction with the Metal−Oxide Interface. J. Am. Chem. Soc. 2017, 139, 5652−5655.
(45) Bigeleisen, J.; Mayer, M. G. Calculation of Equilibrium Constants for Isotopic Exchange Reactions. J. Chem. Phys. 1947, 15, 261−267.
(46) Yan, Y.; Liu, C.; Jian, H.; Cheng, X.; Hu, T.; Wang, D.; Shang, L.; Chen, G.; Schaaf, P.; Wang, X.; Kan, E.; Zhang, T. Substitutionally Dispersed High-Oxidation CoO_x Clusters in the Lattice of Rutile TiO_2 Triggering Efficient Co-Ti Cooperative Catalytic Centers for Oxygen Evolution Reactions. Adv. Funct. Mater. 2021, 31, No. 2009610.
(47) Long, R.; Li, Y.; Liu, Y.; Chen, S.; Zheng, X.; Gao, C.; He, C.; Chen, N.; Qi, Z.; Song, L.; Jiang, J.; Zhu, J.; Xiong, Y. Isolation of Cu Atoms in Pd Lattice: Forming Highly Selective Sites for Photocatalytic Conversion of CO_2 to CH_4. J. Am. Chem. Soc. 2017, 139, 4486−4492.
(48) Wu, W.; Bhattacharyya, K.; Gray, K.; Weitz, E. Photoinduced Reactions of Surface-Bound Species on Titania Nanotubes and Platinized Titania Nanotubes: An in Situ FTIR Study. J. Phys. Chem. C 2013, 117, 20643−20655.
(49) Liu, L.; Zhao, C.; Xu, J.; Li, Y. Integrated CO_2 Capture and Photocatalytic Conversion by a Hybrid Adsorbent/Photocatalyst Material. Appl. Catal., B 2015, 179, 489−499.
(50) Xu, C.; Huang, W.; Li, Z.; Deng, B.; Zhang, Y.; Ni, M.; Cen, K. Photothermal Coupling Factor Achieving CO_2 Reduction Based on Palladium-Nanoparticle-Loaded TiO_2. ACS Catal. 2018, 8, 6582−6593.
(51) Jin, L.; Liu, B.; Louis, M. E.; Li, G.; He, J. Highly Crystalline Mesoporous Titania Loaded with Monodispersed Gold Nanoparticles: Controllable Metal−Support Interaction in Porous Materials. ACS Appl. Mater. Interfaces 2020, 12, 9617−9627.
(52) Hu, M.; Jin, L.; Dang, Y.; Suib, S. L.; He, J.; Liu, B. Supported Pt Nanoparticles on Mesoporous Titania for Selective Hydrogenation of Phenylacetylene. Front. Chem. 2020, 8, No. 581512.
(53) Yang, Y.; Jin, L.; Liu, B.; Kerns, P.; He, J. Direct Growth of Ultrasmall Bimetallic AuPd Nanoparticles Supported on Nitrided Carbon towards Ethanol Electrooxidation. Electrochim. Acta 2018, 269, 441−451.
(54) Ran, J.; Jaroniec, M.; Qiao, S.-Z. Cocatalysts in Semiconductor-Based Photocatalytic CO_2 Reduction: Achievements, Challenges, and Opportunities. Adv. Mater. 2018, 30, No. 1704649.
(55) Trasatti, S. Work Function, Electronegativity, and Electrochemical Behaviour of Metals: III. Electrolytic Hydrogen Evolution in Acid Solutions. J. Electroanal. Chem. Interfacial Electrochem. 1972, 39, 163−184.

https://doi.org/10.1021/acsami.1c09119
ACS Appl. Mater. Interfaces 2021, 13, 38595−38603